IEEE Access
Multidisciplinary | Rapid Review | Open Access Journal

Received March 5, 2020, accepted March 24, 2020, date of publication March 31, 2020, date of current version April 20, 2020.

Digital Object Identifier 10.1109/ACCESS.2020.2984654

An Effective Wind Speed Estimation Based Extended Optimal Torque Control for Maximum Wind Energy Capture

XIAOFEI DENG[1,2,3], JIAN YANG[1,3], (Member, IEEE), YAO SUN[1,3], (Member, IEEE), DONGRAN SONG[1,3], YINGGANG YANG[1,3], AND YOUNG HOON JOO[4]

[1]School of Automation, Central South University, Changsha 410083, China
[2]School of Information Science and Engineering, Jishou University, Jishou 416000, China
[3]Hunan Provincial Key Laboratory of Power Electronics Equipment and Grid, Changsha 410083, China
[4]School of IT Information and Control Engineering, Kunsan National University, Kunsan 573-701, South Korea

Corresponding authors: Xiaofei Deng (xiaofei0228@163.com) and Dongran Song (humble_szy@163.com)

This work was supported in part by the National Natural Science Foundation of China under Grant 51777217 and Grant 61803393, in part by the Project funded by China Postdoctoral Science Foundation under Grant 2017M622605, in part by the Innovation-driven Project of Central South University under Grant 2020CX031, and in part by the Major Project of Changzhutan Self-Dependent Innovation Demonstration Area under Grant 2018XK2002.

ABSTRACT Most variable-speed wind turbines employ advanced control scheme to improve their performance. In this paper, an extended optimal torque controller is designed based on effective wind speed estimation to control the variable-speed wind turbine. To do this, multilayer perceptron based nonlinear input-output mapping is firstly used for approximating the nonlinear aerodynamics of the wind turbine. In other words, based on this nonlinear mapping, effective wind speed is estimated from the measured rotor speed, the measured pitch angle, and the observed aerodynamic torque by the disturbance observer. After that, the optimal rotor speed command for capturing maximum wind energy is derived from the estimated effective wind speed. And then the optimal torque command is calculated by combing the standard optimal torque formula and a proportional control loop that is added to effectively reduce the moment of inertia. At last, some simulation results are validated to display the availability of the improved effective wind speed estimation algorithm and control strategy. Moreover, the corresponding simulation results indicate that compared with the existing methods, the proposed method increases the accuracy of the effective wind speed estimation by 2-7% and the energy production efficiency by 0.35%.

INDEX TERMS Effective wind speed estimator, maximum wind energy capture, extended optimal torque control, variable-speed wind turbine.

NOMENCLATURE

υ_e	effective wind speed
ρ	air density
T_a, P_a	aerodynamic torque and aerodynamic power
C_p	coefficient of aerodynamic power
$C_{p\max}$	maximum power coefficient
λ	tip speed ratio
λ_{opt}	optimal tip speed ratio
R	rotor radius
β	pitch angle
ω_r, ω_g	rotor speed and generator speed
ω_r^*	optimal rotor speed command
s_{dt}, d_{dt}	stiffness and damping coefficient of drive train
J_r, J_g	inertias of blade rotor and generator
T_g	generator torque
T_{sh}, $\frac{T_{sh}}{N}$	low-speed and high-speed shaft torque
N	gearbox ratio
θ_r, θ_g	rotor and generator rotational angles
L	observer gain
F	observer parameter
$\wedge$	estimation
K_p	proportional gain

The associate editor coordinating the review of this manuscript and approving it for publication was Huanqing Wang.

I. INTRODUCTION

Because of a great shortage of conventional energy, renewable energy without pollution has received much interest [1]. Wind energy, as a renewable energy technology, has

received wide attentions [2]–[4]. And variable-speed wind turbine (VSWT) becomes more and more popular due to its high-quality power and high-efficiency power production [5], [6]. In the operating range from cut-in to rated wind speeds, the VSWT can capture maximum wind energy by optimally adjusting the rotor speed. The dominant control method to extract maximum wind energy from VSWT is known as maximum power point tracking control, which mainly consists of two categories [7]: direct power controller and indirect power controller. And this direct power controller straightway maximizes the output electrical power. Though studying the power change on basis of the preformed curve of the system, the direct power controller may give good performance except that the robustness is not guaranteed [8]. The indirect power controller aims at maximizing the extracted mechanical wind energy, by using power signal feedback control [9], tip speed ratio control [10], and optimal torque control (OTC) [11], etc. In [9], the power signal feedback controller is based on the measured power curve of the wind turbine, and this wind turbine seems still not adequate to be installed in complex areas, where the wind turbulence is often very high. In [10], the tip speed ratio controller regulates the rotor speed to maintain the optimal value, but it depends on accurate wind speed information. In [11], an adaptive torque controller is proposed, which seeks the gain that maximizes power capture despite aerodynamic uncertainty and turbulent effects. The disadvantage of the optimal torque control is the slow response for wind variations, resulting in the less energy capture.

To easily implement capturing maximum wind energy, the wind speed information should be provided to improve system performance [12], [13]. Wang *et al.* [12] proposes the advanced light detection and ranging (LIDAR)-enabled controller, which outperforms the baseline optimal torque controller. In this study, the optimal torque control to the wind turbine system combined with a proportional control loop is proposed to decrease the impact of the moment of inertia, which uses the previewed wind speed measured by LIDAR that greatly increases the cost of the system. In reality, most VSWTs employ mechanical anemometers to obtain wind speed information, but these anemometers reduce system performance and increase the equipment and maintenance costs of the VSWT. Therefore, replacing the anemometer with effective wind speed (EWS) estimator on basis of soft computing technique has caused considerable interest all over the world [14].

In the existing literature, there are four categories of the soft computing-based wind speed estimation methods: fuzzy logic model [15], statistical model [16], artificial neural network model [17]–[20], hybrid models [21]–[25]. In [15], a sensorless fuzzy wind speed estimator on basis of fuzzy logic principles heuristically inferred from the typical wind turbine power curve is proposed, but it is trivial to seek out a suitable input limit. In [16], a wind speed estimation method on basis of autoregressive statistical model is presented, but it involves complex computation. In [17], EWS is estimated by using support vector machine, which is only applicable to the problem characterized by nonlinearity, small sample, local minima, high dimension and has high generalization. In [18], a new wind speed estimation way using support vector regression for wind power system is proposed, but it is largely dependent on the wind turbine power without thinking about power losses. In [19], a Gaussian radial basis function network-based wind speed estimation algorithm is proposed. In [20], a sensorless EWS estimation algorithm on the basis of the unknown input disturbance observer and the extreme learning machine (UIDOB-ELM) for the VSWT is presented, but the estimator is not accurate enough at some catastrophe points. Meanwhile, the hybrid techniques, such as adaptive neuro-fuzzy inference system [21], particle swarm optimization based support vector regression approach [22], genetic algorithm based support vector machine model [23], new hybrid metaheuristic model using radial movement optimization and particle swarm optimization [24], have received more attention because of high estimation accuracy. However, the hybrid models are usually complicated and hard to implement in real-time controllers for nonlinear systems.

In recent years, many researchers focus on the modeling and control of nonlinear systems by using advanced methods. In the aspect of modeling, T-S modeling is the current research hotspots [25]–[28]. But the fuzzy gains are not easy to get in wind turbine system application. Up to now, multilayer perceptron (MLP) with simple structure has received much interest in modeling complex nonlinear systems. In [29], a wind speed estimation method for direct-drive small wind turbine generator system based on multilayer perceptron neural network is proposed, which has been verified to be a fast and smooth method. However, this method does not consider energy losses of system. In [30], Velo *et al.* use MLP to determine the annual average wind speed at a complex terrain site. In [31], based on the truck velocity, total resistance and gross vehicle weight, the fuel consumption of haul trucks in surface mines is predicted using the MLP model, which is trained and tested using real data collected from a surface mining operation. And the haul truck fuel consumption can be accurately estimated by the model on the basis of the values of the haulage parameters. Hence, a good idea could be to use MLP approximate the nonlinear aerodynamics of wind turbine, and thus new EWS algorithms may be constructed. In the aspect of control, the advantages of some estimation-based control techniques are clear [32]–[37]. In [32], an observer-based adaptive backstepping decentralized controller is developed by using the approximation capability of radial basis function neural networks. In [33], a systemic fuzzy adaptive control scheme is proposed based on fuzzy approximation property and backstepping technique. In [34], an adaptive fuzzy output feedback controller is proposed based on multi-input and multi-output switched fuzzy observer. In [35], an observer-based adaptive finite-time tracking control scheme is proposed by combining backstepping approach and dynamic surface control technique.

Motivated by the above observations, a novel EWS estimation-based extended optimal torque control (EOTC) scheme is proposed for maximum wind energy capture of VSWT in this study. And the EWS is estimated based on the measured pitch angle, the measured rotor speed and the observed aerodynamic torque.

The wind speed information is vital to improve the real-time advanced control performance, while advanced control could provide more energy capture for the wind turbine. The above situation motivates this study. The achieved contributions can be summarized as follows.

1) The disturbance observer (DOB) is proposed to observe aerodynamic torque, which is simpler and more accurate than the unknown input disturbance observer (UIDOB).
2) The nonlinear MLP mapping is used to estimate the EWS, which is more accurate than the existing estimators.
3) An extended optimal torque controller for tracking the optimal torque command calculated is proposed through using the estimated EWS, which is combined with an added proportional controller to reduce the moment of inertia.

The structure of this article is organized as follows: The wind turbine model and operation are described in Section II. And the EWS estimator based on DOB and MLP (DOB-MLP) and the detailed designs are explained in Section III. Section IV presents the extended optimal torque controller to extract maximum wind energy. And the simulation results are presented in Section V. The conclusions are made in Section VI.

II. WIND TURBINE MODELING AND OPERATION

In this section, the basic of wind turbine model and operation is described.

A. AERODYNAMIC MODELLING OF WIND TURBINE

The aerodynamic model of the wind turbine can be described by power coefficient C_p, which is a function of both the blade pitch angle β and tip speed ratio λ. λ is defined by

$$\lambda = \omega_r R / \upsilon_e \tag{1}$$

where ω_r is the rotor speed, R is the rotor radius, and $_e$ is the rotor EWS.

Given the power coefficient, the aerodynamic torque T_a of the WT is given by [20]

$$T_a = \frac{1}{2\lambda}\rho\pi R^3 C_p(\lambda, \beta)\upsilon_e^2 = \frac{1}{2\lambda^3}\rho\pi R^5 C_p(\lambda, \beta)\omega_r^2 \tag{2}$$

where ρ is the air density.

From (1) and (2), the EWS can be represented as:

$$\upsilon_e = f(T_a, \beta, \omega_r) \tag{3}$$

where $f(\cdot)$ is the nonlinear function characterizing the EWS.

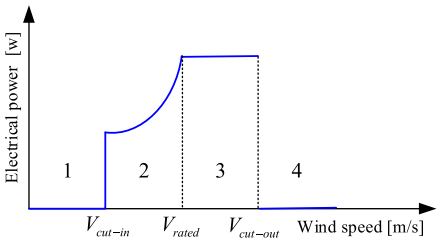

FIGURE 1. Operation regions of WT.

B. SHAFT SYSTEM MODELLING OF WIND TURBINE

The drive train model is represented by a two-mass model [6], [20], [38], where the high-speed generator and low-speed turbine are described by different masses, and the connecting shaft is modeled as a damper and a spring. Therefore, the motion equations are given by [20]

$$\begin{cases} J_r\dot{\omega}_r = T_a - T_{sh} \\ J_g\dot{\omega}_g = T_{sh}/N - T_g \\ T_{sh} = s_{dt}\gamma + d_{dt}\dot{\gamma} \end{cases} \tag{4}$$

where N is gearbox ratio, ω_g is generator rotational speed, T_g is generator torque, and $\gamma = (\theta_r - \theta_g/N)$; θ_g and θ_r are generator and rotor rotational angles, respectively; J_g and J_r are the inertia moment of the generator and the rotor, respectively; T_{sh}/N and T_{sh} are the high-speed and low-speed shaft torque, respectively; s_{dt} is the stiffness coefficient of the flexible coupling between the two masses, and d_{dt} is the shaft damping.

C. OPERATION OF WIND TURBINE

As indicated in Figure 1, the operation of wind turbine includes four operating regions:

Region 1, in which the wind turbine cannot operate normally, the range of wind speed is 0-3 m/s for the wind turbine in a general case.

Region 2, in which the wind turbine operates from cut-in to rated wind speeds, the optimal rotor speed is obtained and the maximum wind energy is extracted (also called partial load), the range is 3-10.9 m/s. In this paper, only Region 2 is considered.

Region 3, between rated and cut-out wind speeds, where the turbine must limit the captured wind energy for safety, the rotor speed is maintained at rated value through pitching the blades (also called full load), and the range of wind speed is 10.9-25m/s.

Region 4, in which the wind turbine is turned out to prevent the wind turbine from being damaged, the range is above cut-out wind speed 25m/s.

III. ESTIMATION OF EFFECTIVE WIND SPEED

In this section, the DOB-based aerodynamic torque estimator and MLP mapping are detailed.

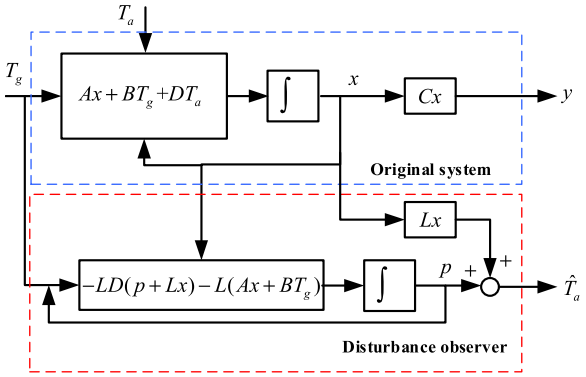

FIGURE 2. Block diagram of the disturbance observer.

A. DISTURBANCE OBSERVER BASED AERODYNAMIC TORQUE ESTIMATION

To make it easier to design the aerodynamic torque observer, the two-mass drive train model (4) can be represented as the state-space model:

$$\begin{cases} \dot{x} = Ax + BT_g + DT_a \\ y = Cx \end{cases} \tag{5}$$

where the system matrix is presented as:

$$\mathrm{A} = \begin{bmatrix} 0 & 1 & -1/N \\ -s_{dt}/J_r & -d_{dt}/J_r & d_{dt}/(J_r N) \\ s_{dt}/(J_g N) & d_{dt}/(J_g N) & -d_{dt}/(J_g N^2) \end{bmatrix},$$
$$C = \begin{bmatrix} 0 & 1 & 0 \end{bmatrix},$$
$$B = \begin{bmatrix} 0 & 0 & -1/J_g \end{bmatrix}^T, \quad D = \begin{bmatrix} 0 & 1/J_r & 0 \end{bmatrix}^T.$$

And the state is represented as $x = [\gamma, \omega_r, \omega_g]^T$.

Besides, the rotor speed ω_r and the generator torque T_g can be measured. And the measured rotor speed ω_r is also the input of the following MLP algorithm.

For the system described in (5), the aerodynamic torque T_a is considered as the disturbance input, the following DOB [39] is given by

$$\begin{cases} \dot{p} = -LD(p + Lx) - L(Ax + BT_g) \\ \hat{T}_a = p + Lx \end{cases} \tag{6}$$

where $\hat{T}_a$ is the disturbance estimate, p is an auxiliary vector and L is the observer gain matrix to be designed.

The structure of the DOB is shown in Figure 2, in which the disturbance input T_a is estimated. According to (5), the original system is obtained. Then, based on (6), the DOB is got.

It can be derived from the DOB (6) that

$$\dot{\hat{T}}_a = LD(T_a - \hat{T}_a) \tag{7}$$

If the estimation error of the disturbance is $e_1 = T_a - \hat{T}_a$, the dynamic characteristics of disturbance estimation is as follows.

$$\dot{e}_1 = \dot{T}_a - LDe_1 \tag{8}$$

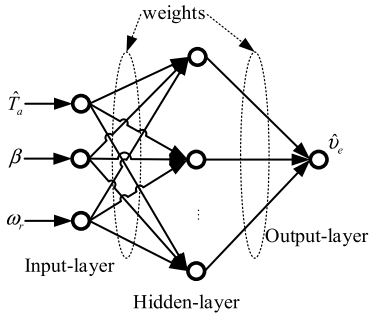

FIGURE 3. Structure of the MLP-based effective wind speed estimator.

The observer gain L is designed as follows: $L = F(D^T D)^{-1} D^T$, where F is the observer parameter, and the observer gain L is chosen such that $F > 0$ holds. Thus, we can derive the dynamics of the DOB as:

$$\dot{e}_1 = \dot{T}_a - Fe_1 \tag{9}$$

when F is given, the disturbance input T_a is observed. The observed $\hat{T}_a$ will be used as the input of following MLP model.

B. MULTILAYER PERCEPTRON BASED EFFECTIVE WIND SPEED ESTIMATION

Given the information of the aerodynamic torque T_a, the blade pitch angle β and the rotor speed ω_r, the EWS can be figured out from the nonlinear inverse function of (2). However, searching for the solution of nonlinear inverse function may be time-consuming and reduce system performance. A novel method to resolving this trouble is using ELM algorithm [20]. But this estimator estimates imprecisely at some catastrophe points. Therefore, MLP instead of ELM algorithm is used to estimate the EWS in this paper.

In addition, the nonlinear function (2) can be expressed as (3). Therefore, the proposed EWS estimation method is on the basis of the MLP-based input-output mapping, which is capable of approximating the nonlinear function (3). MLP in most applications covers feedforward neural networks with one input layer, one hidden layer, and one output layer. And the MLP-based EWS estimation model has three inputs ($\hat{T}_a$, β, ω_r) and one output $\hat{v}_e$, as presented in Figure 3.

The input-output mapping for MLP is given by:

$$y_p^{(k)} = gaussian_p^{(k)} \left[\sum_{i=1}^{N_{k-1}} W_{ip}^{(k-1)} \cdot y_i^{(k-1)} - b_p^{(k)} \right],$$
$$p = 1, 2, \cdots, N_k; \quad k = 1, 2, \cdots, M \tag{10}$$

where $W_{ip}^{(k-1)}$ is the weight vector connecting the ith node in the $(k-1)$th layer and the pth node in the kth layer, $y_i^{(k-1)}$ is the output of the ith node in the $(k-1)$th layer, $y_p^{(k)}$ is the output of the pth node in the kth layer, $b_p^{(k)}$ is the threshold of the pth node in the kth layer, and $gaussian_p{}^{(k)}$ is the gaussian activation function of the pth node in the kth layer.

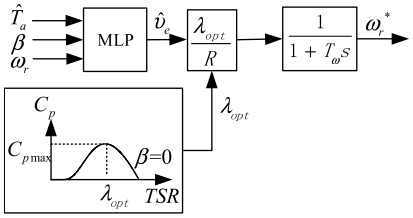

FIGURE 4. Block diagram of the MLP-based optimal rotor speed estimator.

Gaussian activation function can be expressed as:

$$gaussian(x) = e^{-x^2/2\sigma^2} \tag{11}$$

where σ is a parameter whose value controls the smoothness properties of the activation function.

In this paper, the learning rule used is generalized delta rule. Then weights are updated on the basis of the errors between the desired and model output. And the algorithm step is given by [40]:

Step 1: Initialization randomly.

Step 2: Calculating the output vector.

Step 3: Calculating the error propagation terms.

Step 4: Updating the weights with (12).

Step 5: Calculating the total error ε_{total} with (13).

Step 6: Iterating the calculation by going back to Step 2 until the total error is less than the desired error.

$$W_{ip}^{(k-1)}(t+1) = W_{ip}^{(k-1)}(t) + \psi \sum_{n=1}^{I} \delta_{np}^{(k)} y_{ni}^{(k-1)} \tag{12}$$

where $\delta_{np}^{k} = gaussian_{np}^{(k)}(\cdot) \cdot \left[\sum_{l=1}^{N_{k+1}} \delta_{nl}^{(k+1)} W_{pl}^{(k)}(t) \right]$, ψ is the learning rate and t is the number of iterations.

$$\varepsilon_{total} = \sum_{n=1}^{I} \sum_{j=1}^{N_M} \left(y_{nj}^{(M)} - \hat{y}_{nj}^{(M)} \right)^2 \tag{13}$$

where ε_{total} is the total error, $y_{nj}^{(M)}$ is the desired output, $\hat{y}_{nj}^{(M)}$ is the model output.

IV. EXTENDED OPTIMAL TORQUE CONTROL FOR MAXIMUM WIND ENERGY CAPTURE

In this section, the Multilayer perceptron based sensorless optimal rotor speed estimation and the extended optimal torque control are elaborated.

A. MULTILAYER PERCEPTRON BASED SENSORLESS OPTIMAL ROTOR SPEED ESTIMATION

In Region 2, the rotor speed of the wind turbine is bound to attain an optimal tip speed ratio λ_{opt}, and the optimal command ω_r^* is calculated by

$$\omega_r^* = \lambda_{opt} \hat{\upsilon}_e / R \tag{14}$$

Figure 4 shows the structure of the MLP-based optimal rotor speed estimator. As known to all, wind speed often varies randomly and quickly, but the wind turbine is relatively slow in response because of the inertia. Hence, a low pass filter is indispensable, which is added to offer the smooth optimal rotor speed reference to the wind turbine.

B. EXTENDED OPTIMAL TORQUE CONTROL

On the basis of ω_r^*, the value of the generator torque reference is expressed as [41]

$$T_g^* = K_{opt}(\omega_r^*)^2 \tag{15}$$

where $K_{opt} = \frac{\rho \pi R^5 C_{p\max}}{2N(\lambda_{opt})^3}$.

At the stable running operating point, the aerodynamic torque of the drive train model (3) can be linearized, which is given by [41], [42]

$$(J_r + J_g)\frac{d\delta\omega_r}{dt} \approx \delta T_a - N\delta T_g \tag{16}$$

In the optimal torque control, the generator torque reference can also be linearized at the stable running operating point, which is given by [41], [42]

$$\begin{aligned} T_g^* &= T_{g0} + \delta T_g \\ &= K_{opt}(\omega_{r0} + \delta\omega_r)^2 \\ &\approx K_{opt}{\omega_{r0}}^2 + 2K_{opt}\omega_{r0}\delta\omega_r \end{aligned} \tag{17}$$

where ω_{r0} and T_{g0} are the rotor speed and the generator torque at the stable operating point, respectively. At the stable operating point of optimal torque control, the value of $\delta\omega_r$ is extremely small, and its square value is even smaller. Therefore, the term with the square value is approximately equal to 0, and the formula (17) holds. From (16) and (17), the transfer function between the rotor speed and the aerodynamic torque is given by [41]

$$G(s) = \frac{\delta\omega_r}{\delta T_a} = \frac{1}{(J_r + J_g)s + 2NK_{opt}\omega_{r0}} \tag{18}$$

To improve the transient performance of the optimal torque control, the discrepancy between the generator torque and the aerodynamic torque should be big, which results in the rapid deceleration or acceleration of the wind turbine system. Besides, the optimal torque controller must keep the C_{pmax} at the steady state. By adding a proportional controller, the performance of the optimal torque controller can meet the control requirements aforementioned [41]. With the added proportional control loop, the transfer function in (18) is rewritten as [41]

$$G'(s) = \frac{\delta\omega_r}{\delta T_a} = \frac{1}{\frac{(J_r+J_g)}{(1+K_p)}s + 2NK_{opt}\omega_{r0}} \tag{19}$$

where K_p is a proportional gain. And this proportional gain affects the transient performance of the extended optimal torque controller. From (19), the dynamic response becomes faster, and the reason is that the inertias of J_r and J_g are decreased by the proportional gain.

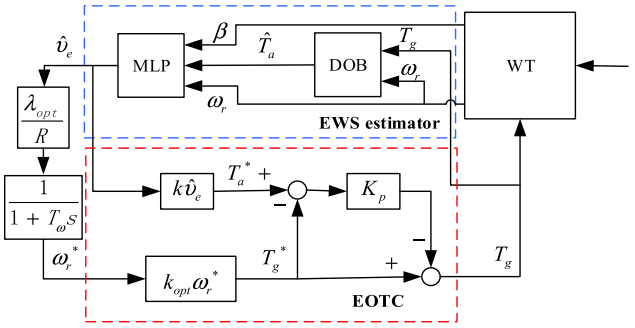

FIGURE 5. Block diagram of the extended optimal torque controller.

In addition, from (2), the aerodynamic torque T_a^* can be calculated according to the estimated EWS, which is expressed as

$$T_a^*(=T_a) = k\hat{v}_e^2 \tag{20}$$

where $k = \rho\pi R^3 C_{p\max}/2N\lambda_{opt}$. The proposed extended optimal torque control scheme is given by

$$T_g = K_{opt}(\omega_r^*)^2 - K_p[k\hat{v}_e^2 - K_{opt}(\omega_r^*)^2] \tag{21}$$

Nevertheless, the gain K_p should be carefully selected because the practical wind turbine system has physical limitations. In this paper, the gain K_p is selected as 0.9 by trial and error.

This control algorithm has the ability of reducing the influences of the inertia moment [41]. Based on the well-known optimal torque algorithm, the general controller consists of two parts. The first part is the proposed EWS estimator, and the second part is the EOTC. Therefore, the general structure of the proposed extended optimal torque controller is given by Figure 5.

C. IMPLEMENTATION OF THE EXTENDED OPTIMAL TORQUE CONTROLLER

The implementation steps of the developed controller in application are shown in Figure 6. Firstly, measuring the generator torque, pitch angle, and rotor speed. Secondly, estimating the aerodynamic torque by DOB based on the measured generator torque and the rotor speed. The observer parameters are calculated offline. Thirdly, the EWS is got by the MLP model trained offline according to the information of the aerodynamic torque, pitch angle, and rotor speed. Finally, the optimal torque command is calculated to control the wind turbine. The developed controller is actually a little more complicated than OTC. However, the execution time of the EWS-based wind turbine controller used in engineering is merely related to the online running part, and the offline calculating and training parts of the EWS estimator are not included. Therefore, the developed controller does not affect the real-time operation of the control system.

V. SIMULATION STUDY

The proposed method is tested on the industry-standard Bladed design software [43] and the MATLAB software.

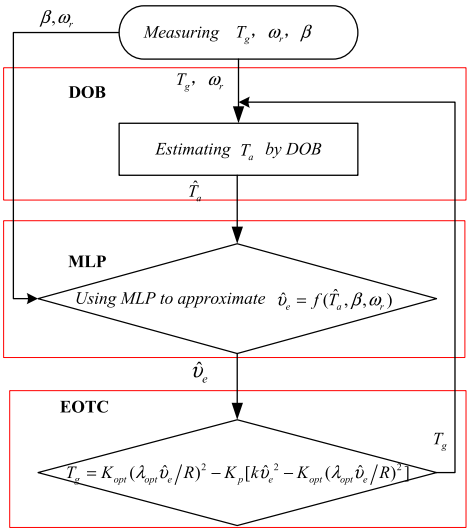

FIGURE 6. Flowchart of the extended optimal torque controller.

TABLE 1. Parameters of the concerned wind turbine.

Parameter	Value
Rated electrical power	1500 kW
Optimal TSR	9.5
Maximum power coefficient	0.483
Drive train damping coefficient	1.0×10^4 N·m·s/rad
Drive train stiffness coefficient	1.38×10^8N·m/rad
Air density	1.225 kg/m^3
Rotor radius	41m
Gearbox ratio	100.48
Generator moment of inertia	92 kg·m^2
Rotor moment of inertia	4.94×10^6 kg·m^2

Some simulation results about performance comparisons with classical and novel method will be provided. Detailed wind turbine model is available via Bladed to simulate the operation of a 1.5 MW, three-blade, VSWT, which is manufactured by the China Ming Yang Smart Energy, and the specifications are stated in Table 1 [44]–[46].

A. VALIDATION OF THE DISTURBANCE OBSERVER

It is worth mentioning that the disturbance observer parameter after tuning is set as $F = 1700$. The mean wind speed is selected among 3-10.9 m/s because only Region 2 is considered. For simplicity, two representative simulation results are selected, namely, 4 m/s and 8 m/s.

The relative estimation error ε_r is employed to evaluate the DOB's performance, which is given by [47]:

$$\varepsilon_r = \frac{T_a(t) - \hat{T}_a(t)}{T_a(t)} \tag{22}$$

And then their statistical properties are used to assess the performance of the DOB [20]. In addition, Table 2 summarizes the statistical comparisons between the DOB and the UIDOB. As indicated in Table 2, the results of $E[|\varepsilon_r|]$ for UIDOB and DOB are 0.0030912 and 0.0010688

TABLE 2. Comparisons for the two observers about statistical properties.

Param	UIDOB (4 m/s)	DOB (4 m/s)	UIDOB (8 m/s)	DOB (8 m/s)
$E\left[\left\|\varepsilon_r\right\|\right]$	0.0030912	0.0010688	0.0014502	0.0009194
σ_{ε_r}	0.0799289	0.0076334	0.0072383	0.0072170
CC	0.9999263	0.9999487	0.9995417	0.9995424

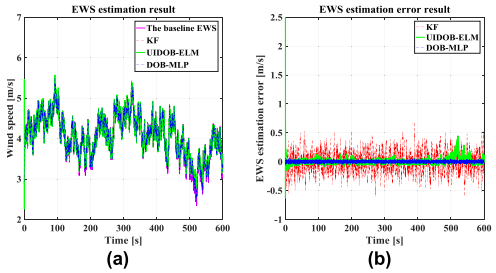

FIGURE 7. Estimation results of effective wind speed at 4 m/s mean wind speed. (a) Comparisons between the baseline and the three estimators. (b) Comparisons of three absolute estimation errors.

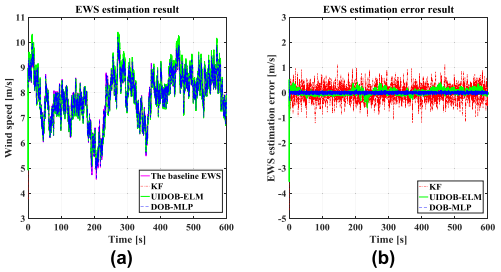

FIGURE 8. Estimation results of effective wind speed at 8 m/s mean wind speed. (a) Comparisons between the baseline and the three estimators. (b) Comparisons of three absolute estimation errors.

TABLE 3. Comparisons for the two observers about statistical properties.

Param	UIDOB-ELM (4 m/s)	DOB- MLP (4 m/s)	UIDOB-ELM (8 m/s)	DOB- MLP (8 m/s)
$E\left[\left\|\varepsilon\right\|\right]$	0.0274704	0.0033654	0.0680544	0.0049361
σ_{ε}	0.0517679	0.0061566	0.0996955	0.0122540
CC	0.9956889	0.9999275	0.9955535	0.9999162

at 4 m/s, respectively. And the results are 0.0014502 and 0.0009194 at 8 m/s, respectively. Moreover, the results of $\sigma_{\varepsilon r}$ are 0.0799289 and 0.0076334 at 4 m/s, respectively. And the results are 0.0072383 and 0.0072170 at 8 m/s, respectively. Therefore, all $E[|\varepsilon_r|]$ and $\sigma_{\varepsilon r}$ results of the DOB less than the ones of the UIDOB, show that the observation error of DOB is smaller. In addition, the Correlation Coefficients (CC) results of UIDOB and DOB are 0.9999263 and 0.9999487 at 4 m/s, respectively. And the results are 0.9995417 and 0.9995424 at 8 m/s, respectively. That is, all CC results of DOB are closer to 1.0 than the ones of the UIDOB. Obviously, the DOB estimates more accurately. Besides, the structure of the DOB is easier and simpler to implement, the reason is that there is only one observer parameter to be tuned. However, two parameters, namely proportional gain and integral gain, need to be tuned for the UIDOB. Hence, the comprehensive performance of the DOB is superior to that of the UIDOB.

B. VALIDATION OF THE EFFECTIVE WIND SPEED ESTIMATOR

1) RESULTS OF THE EFFECTIVE WIND SPEED ESTIMATORS

The EWS is estimated by the MLP algorithm (Figure 3), using the measured pitch angle, the measured rotor speed, and the previous observed aerodynamic torque as inputs. And the model is trained offline, with 8 neurons in the hidden layer. The activation function of the hidden layer and the output layer is gaussian function. The parameters of the MLP are updated by using the error between the reference model and the MLP output. The desired error is set as 1e-6.

Then, a comparison is carried out with the UIDOB-ELM estimator [20] and the Kalman filter (KF) based estimator [48] to verify the validity of the improved estimator. It should be noticed that two representative estimation results are shown in Figures 7-8, namely 4 m/s and 8 m/s.

Figures 7-8(a) show the results of estimated EWS, and Figures 7-8(b) show the results of the absolute EWS estimation error. As shown in Figures 7-8(a), there are similar trends among the three EWS estimators, so all estimators work properly. However, difference remains clear, as shown in Figures 7-8(b), the estimation errors of the DOB-MLP estimator, the UIDOB-ELM estimator and the KF-based estimator are kept within ± 0.15 m/s, ± 0.2 m/s, and ± 0.5 m/s, respectively. In other words, the absolute estimation errors of the KF-based estimator are larger than those of the other two estimators. The reason is that the KF-based estimator is not suitable for nonlinear function approximation. Although, the errors of the UIDOB-ELM estimator are much smaller than those of the KF-based estimator, the UIDOB-ELM estimator fails in precisely estimating the EWS for some peak and valley points, especially at the start. Therefore, it is obvious that the proposed DOB-MLP estimator works more accurately in the whole operation process.

2) RESULTS OF STATISTICAL PROPERTIES

In order to evaluate the improved EWS estimator, the absolute estimation error ε is selected, which is given by [20]:

$$\varepsilon = \upsilon_e - \hat{\upsilon}_e \tag{23}$$

Besides, the statistical properties are used to evaluate performance of the improved EWS estimator as well [20]. Moreover, Table 3 summarizes the statistical comparisons between the UIDOB-ELM estimator and DOB-MLP estimator. And Table 3 shows that all $E[|\varepsilon|]$ and σ_{ε} results of the proposed estimator are less than the ones of the UIDOB-ELM estimator, and all CC results are greater. Of course, it also means that the DOB-MLP estimator outperforms the UIDOB-ELM estimator.

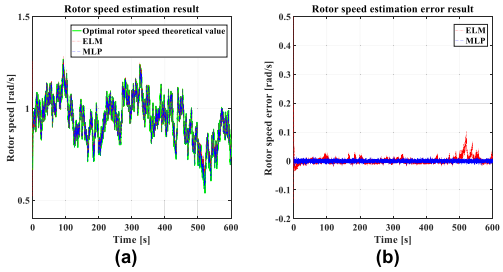

FIGURE 9. Estimation results of optimal rotor speed at 4 m/s mean wind speed. (a) Comparisons between the optimal rotor speed of theoretical value and the two estimators. (b) The two optimal rotor speed absolute estimation errors.

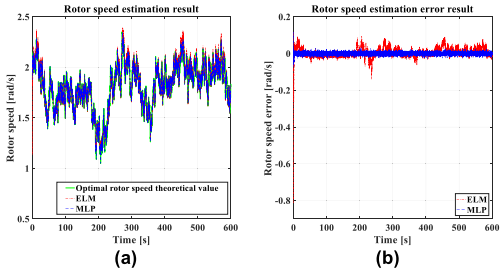

FIGURE 10. Estimation results of optimal rotor speed at 8 m/s mean wind speed. (a) Comparisons between the optimal rotor speed of theoretical value and the two estimators. (b) The two optimal rotor speed absolute estimation errors.

C. VALIDATION OF THE EXTENDED OPTIMAL TORQUE CONTROLLER

1) RESULTS OF THE OPTIMAL ROTOR SPEED ESTIMATOR

Based on the EWS, the optimal rotor speed command ω_r^* for maximum wind energy extraction is determined. Then the simulation results for the optimal rotor theoretical value, the ELM estimator, and the MLP estimator are presented in Figures 9-10.

Figures 9-10(a) show that the estimated rotor speed tracks its theoretical value well. The tracking errors of the MLP estimator are almost kept within ± 0.03 rad/s, and the main tracking errors of the ELM estimator are kept within ± 0.1 rad/s, as shown in Figures 9-10(b). It's obvious that the proposed MLP estimator is more superior with less tracking error. It should be noted that there are large fluctuations in the tracking results of the ELM estimator, that is, it fails in tracking its theoretical value for some operation points, such as peak and valley points, and the start points. Moreover, the tracking results of the proposed MLP estimator are much flatter.

2) RESULTS OF THE EXTENDED OPTIMAL TORQUE CONTROLLER

Up to now, OTC is still the main control scheme to capture the maximum wind energy in industrial application. To verify the validity of EOTC, the comparison with the well-known OTC is carried out. To evaluate the performance of maximum wind energy capture, the value of rotor speed absolute

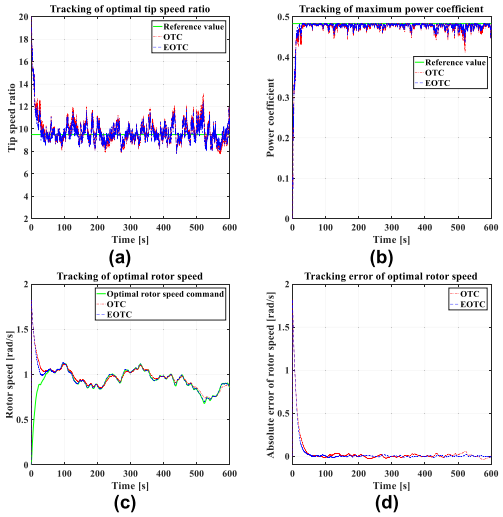

FIGURE 11. The tracking results of OTC and EOTC at 4 m/s mean wind speed. (a) Tracking of optimal tip speed ratio for OTC and EOTC. (b) Tracking of maximum power coefficient for OTC and EOTC. (c) Tracking of optimal rotor speed for OTC and EOTC. (d) Tracking error of optimal rotor speed for OTC and EOTC.

tracking error ε_ω is selected, which is given by

$$\varepsilon_\omega = \omega_r - \omega_r^* \tag{24}$$

For the sake of simplicity, the representative simulation results of 4 m/s are selected. The mean absolute deviation $E[|\varepsilon_\omega|]$ for OTC and EOTC is 0.0484068 and 0.0377499, respectively. The standard deviation of the tracking error $\sigma_{\varepsilon\omega}$ for OTC and EOTC is 0.1757097 and 0.1739519, respectively. What is more, the CC between the optimal rotor command and the tracking value for OTC and EOTC are 0.9854477 and 0.9971686, respectively. Therefore, the tracking performance of EOTC is better than that of OTC.

The simulation results of the comparisons for OTC and EOTC are shown in Figures 11-12, telling that EOTC gives faster response than OTC.

Figure 11(a) shows the comparison of tracking the optimal tip speed ratio between OTC and EOTC. Although both values fluctuate around the reference value, EOTC works better than OTC clearly. Then, the comparison of tracking the maximum power coefficient between the two methods is shown in Figure 11(b), and EOTC has better tracking performance than OTC. In Figure 11(c), the comparison of tracking the optimal rotor speed is presented as well. It is easy to get the conclusion that the proposed EOTC is effective, and the error margin is smaller as dedicated in Figure 11(d). Figure 11(d) shows that the main tracking errors of EOTC are kept within ± 0.02 rad/s, and the main tracking errors of OTC are kept within ± 0.04 rad/s.

Figure 12(a) shows the electrical power comparison for OTC and EOTC. Moreover, EOTC produces more electrical power than OTC as indicated in Figure 12(b). And the average values of electrical power gain for OTC and EOTC are 9.878709 kW and 9.913138 kW, respectively.

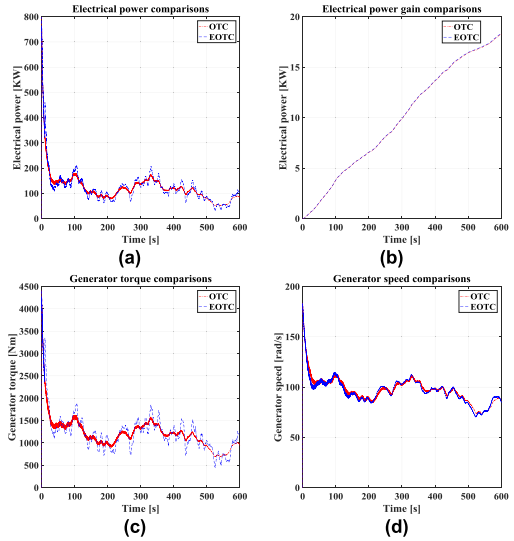

FIGURE 12. **The comparisons of electrical power, generator torque and speed at 4 m/s mean wind speed. (a) Electrical power comparison for OTC and EOTC. (b) Electrical power gain comparison for OTC and EOTC. (c) Generator torque comparison for OTC and EOTC. (d) Generator speed comparison for OTC and EOTC.**

Figure 12(c) shows the generator torque comparison for OTC and EOTC. It is obvious that OTC produces flatter generator torque compared to EOTC. And the average values of generator torque for OTC and EOTC are 1214.16898 Nm and 1222.69419 Nm, respectively. Figure 12(d) shows the generator speed comparison for OTC and EOTC. It is obvious that EOTC responses faster than OTC. From Figure 12(a) and (c), the fluctuations of EOTC are more obvious than OTC. Simply speaking, this is mainly caused by the inner resonance of the wind turbine drive train system.

VI. CONCLUSION AND FUTURE WORK

In this paper, a DOB-MLP based EWS estimator has been proposed for the wind turbine. And then an optimal rotor speed estimator based on EWS estimation has been put forward. Multilayer perceptron is used to map the nonlinear characteristics of wind turbine. That is, the EWS is estimated from the nonlinear multilayer perceptron mapping, and then the optimal rotor speed is determined from the estimated EWS. At last, an extended optimal torque controller based on the estimated EWS and optimal rotor speed is proposed.

Simulation tests have been conducted on the 1.5 MW wind turbine, validating the improved EWS estimator, optimal rotor speed estimator and extended optimal torque controller. To evaluate the performance of the improved EWS estimator, the simulation results have been compared with KF-based and UIDOB-ELM estimators. And the estimation accuracy of the improved estimator is within ± 0.15 m/s, which is superior to that of the UIDOB-ELM estimator within ± 0.2 m/s, and that of the KF-based estimator within ± 0.5 m/s. That is, the accuracy of the proposed method is improved by 2-7% compared with the UIDOB-ELM estimator.

In addition, the simulation results have been compared with the extreme learning machine estimator to evaluate the performance of the optimal rotor speed estimator. The estimation accuracy of the proposed multilayer perceptron optimal rotor speed estimator within ± 0.03 rad/s is superior to that of the extreme learning machine estimator within ± 0.1 rad/s. Then the proposed extended optimal torque control is proved to outperform the well-known optimal torque control, as the error margin of tracking the optimal rotor speed for extended optimal torque control is ± 0.02 rad/s, which is 0.02 rad/s smaller than that of optimal torque control. And the average electrical power for extended optimal torque control improves the energy production efficiency by 0.35%.

However, the precise tracking of the rotor speed and the higher wind energy capture efficiency are at the expense of the variations of the generator torque and electrical power. Hence, avoiding inner resonance to resolve this conflict and improving the performance of maximum wind energy extraction are the biggest challenges we are facing. In future work, we shall consider avoiding inner resonance by reducing the torsional vibration of the drive train. The modification of the existing method to improve the energy production efficiency will also be studied. In addition, the parameters estimation could be an important direction, which will be also studied in our future work.

REFERENCES

[1] X. Lü, Y. Qu, Y. Wang, C. Qin, and G. Liu, "A comprehensive review on hybrid power system for PEMFC-HEV: Issues and strategies," *Energy Convers. Manage.*, vol. 171, pp. 1273–1291, Sep. 2018.

[2] X. Wu and Y. Jiang, "Source-Network-Storage joint planning considering energy storage systems and wind power integration," *IEEE Access*, vol. 7, pp. 137330–137343, 2019.

[3] J. Li, Y. Fu, Z. Xing, X. Zhang, Z. Zhang, and X. Fan, "Coordination scheduling model of multi-type flexible load for increasing wind power utilization," *IEEE Access*, vol. 7, pp. 105840–105850, 2019.

[4] D. Song, X. Fan, J. Yang, A. Liu, S. Chen, and Y. H. Joo, "Power extraction efficiency optimization of horizontal-axis wind turbines through optimizing control parameters of yaw control systems using an intelligent method," *Appl. Energy*, vol. 224, pp. 267–279, Aug. 2018.

[5] H. Ren, H. Zhang, H. Zhou, P. Zhang, X. Lei, G. Deng, and B. Hou, "A novel constant output powers compound control strategy for variable-speed variable-pitch wind turbines," *IEEE Access*, vol. 6, pp. 17050–17059, 2018.

[6] D. R. Song, J. Yang, Z. L. Cai, M. Dong, M. Su, and Y. H. Wang, "Wind estimation with a non-standard extended Kalman filter and its application on maximum power extraction for variable speed wind turbines," *Appl. Energy*, vol. 190, pp. 670–685, Mar. 2017.

[7] D. Kumar and K. Chatterjee, "A review of conventional and advanced MPPT algorithms for wind energy systems," *Renew. Sustain. Energy Rev.*, vol. 55, pp. 957–970, Mar. 2016.

[8] Q. H. Zhong, Y. Ruan, M. H. Zhao, and L. Tian, "Application of variable-step hill climbing searching in maximum power point tracking for DFIG wind power generation system," *Dianli Xitong Baohu yu Kongzhi/Power Syst. Prot Control*, vol. 41, no. 9, pp. 67–73, Apr. 2013.

[9] L. C. Pagnini, M. Burlando, and M. P. Repetto, "Experimental power curve of small-size wind turbines in turbulent urban environment," *Appl. Energy*, vol. 154, pp. 112–121, Sep. 2015.

[10] K. E. Johnson, L. Y. Pao, M. J. Balas, and L. J. Fingersh, "Control of variable-speed wind turbines: Standard and adaptive techniques for maximizing energy capture," *IEEE Control Syst. Mag.*, vol. 26, no. 3, pp. 70–81, Jun. 2006.

[11] M. Cheng and Y. Zhu, "The state of the art of wind energy conversion systems and technologies: A review," *Energy Convers. Manage.*, vol. 88, pp. 332–347, Dec. 2014.

[12] N. Wang, K. E. Johnson, and A. D. Wright, "Comparison of strategies for enhancing energy capture and reducing loads using LIDAR and feedforward control," *IEEE Trans. Control Syst. Technol.*, vol. 21, no. 4, pp. 1129–1142, Jul. 2013.
[13] A. B. Asghar and X. Liu, "Adaptive neuro-fuzzy algorithm to estimate effective wind speed and optimal rotor speed for variable-speed wind turbine," *Neurocomputing*, vol. 272, pp. 495–504, Jan. 2018.
[14] D. Song, Y. Yang, S. Zheng, X. Deng, J. Yang, M. Su, W. Tang, X. Yang, L. Huang, and Y. H. Joo, "New perspectives on maximum wind energy extraction of variable-speed wind turbines using previewed wind speeds," *Energy Convers. Manage.*, vol. 206, Feb. 2020, Art. no. 112496.
[15] A. Naba, F. o. M. Study Program of InstrumentationDepartment of Physics, I. Natural Sciences University of Brawijaya Jl. VeteranMalangEast Java 65145, and A. Nadhir, "Power curve based-fuzzy wind speed estimation in wind energy conversion systems," *J. Adv. Comput. Intell. Intell. Informat.*, vol. 22, no. 1, pp. 76–87, Jan. 2018.
[16] K. Tan and S. Islam, "Optimum control strategies in energy conversion of PMSG wind turbine system without mechanical sensors," *IEEE Trans. Energy Convers.*, vol. 19, no. 2, pp. 392–399, Jun. 2004.
[17] X. Yang, X. Han, L. Xu, and Y. Liu, "Soft sensor based on support vector machine for effective wind speed in large variable wind," in *Proc. 9th Int. Conf. Control, Autom., Robot. Vis.*, 2006, p. 919.
[18] A. G. Abo-Khalil and D.-C. Lee, "MPPT control of wind generation systems based on estimated wind speed using SVR," *IEEE Trans. Ind. Electron.*, vol. 55, no. 3, pp. 1489–1490, Mar. 2008.
[19] W. Qiao, W. Zhou, J. M. Aller, and R. G. Harley, "Wind speed estimation based sensorless output maximization control for a wind turbine driving a DFIG," *IEEE Trans. Power Electron.*, vol. 23, no. 3, pp. 1156–1169, May 2008.
[20] X. Deng, J. Yang, Y. Sun, D. Song, X. Xiang, X. Ge, and Y. H. Joo, "Sensorless effective wind speed estimation method based on unknown input disturbance observer and extreme learning machine," *Energy*, vol. 186, Nov. 2019, Art. no. 115790.
[21] S. Shamshirband, D. Petković, N. B. Anuar, M. L. Mat Kiah, S. Akib, A. Gani, Ž. Ćojbašić, and V. Nikolić, "Sensorless estimation of wind speed by adaptive neuro-fuzzy methodology," *Int. J. Electr. Power Energy Syst.*, vol. 62, pp. 490–495, Nov. 2014.
[22] A. G. Abo-Khalil, S. Alyami, K. Sayed, and A. Alhejji, "Dynamic modeling of wind turbines based on estimated wind speed under turbulent conditions," *Energies*, vol. 12, no. 10, 2019, Art. no. 1907.
[23] D.-Y. Li, W.-C. Cai, P. Li, Z.-J. Jia, H.-J. Chen, and Y.-D. Song, "Neuroadaptive variable speed control of wind turbine with wind speed estimation," *IEEE Trans. Ind. Electron.*, vol. 63, no. 12, pp. 7754–7764, Dec. 2016.
[24] A. Kerem and A. Saygin, "Scenario-based wind speed estimation using a new hybrid metaheuristic model: Particle swarm optimization and radial movement optimization," *Meas. Control*, vol. 52, nos. 5–6, pp. 493–508, Jun. 2019.
[25] X.-H. Chang and G.-H. Yang, "Nonfragile H_∞ filter design for T–S fuzzy systems in standard form," *IEEE Trans. Ind. Electron.*, vol. 61, no. 7, pp. 3448–3458, Jul. 2014.
[26] X.-H. Chang, J. Xiong, and J. H. Park, "Estimation for a class of parameter-controlled tunnel diode circuits," *IEEE Trans. Syst., Man, Cybern. Syst.*, early access, Aug. 13, 2018, doi: 10.1109/TSMC.2018.2859933.
[27] Y. Wang, X. Yang, and H. Yan, "Reliable fuzzy tracking control of near-space hypersonic vehicle using aperiodic measurement information," *IEEE Trans. Ind. Electron.*, vol. 66, no. 12, pp. 9439–9447, Dec. 2019.
[28] X.-H. Chang and G.-H. Yang, "Nonfragile H_∞ filtering of continuous-time fuzzy systems," *IEEE Trans. Signal Process.*, vol. 59, no. 4, pp. 1528–1538, Apr. 2011.
[29] H. Li, K. L. Shi, and P. G. McLaren, "Neural-Network-Based sensorless maximum wind energy capture with compensated power coefficient," *IEEE Trans. Ind. Appl.*, vol. 41, no. 6, pp. 1548–1556, Nov. 2005.
[30] R. Velo, P. López, and F. Maseda, "Wind speed estimation using multilayer perceptron," *Energy Convers. Manage.*, vol. 81, pp. 1–9, May 2014.
[31] A. Soofastaei, S. M. Aminossadati, M. M. Arefi, and M. S. Kizil, "Development of a multi-layer perceptron artificial neural network model to determine haul trucks energy consumption," *Int. J. Mining Sci. Technol.*, vol. 26, no. 2, pp. 285–293, Mar. 2016.
[32] H. Wang, P. X. Liu, J. Bao, X.-J. Xie, and S. Li, "Adaptive neural output-feedback decentralized control for large-scale nonlinear systems with stochastic disturbances," *IEEE Trans. Neural Netw. Learn. Syst.*, vol. 31, no. 3, pp. 972–983, Mar. 2020.
[33] H. Wang, P. Xiaoping Liu, X. Xie, X. Liu, T. Hayat, and F. E. Alsaadi, "Adaptive fuzzy asymptotical tracking control of nonlinear systems with unmodeled dynamics and quantized actuator," *Inf. Sci.*, Apr. 2018, doi: 10.1016/j.ins.2018.04.011.
[34] X. Huo, L. Ma, X. Zhao, B. Niu, and G. Zong, "Observer-based adaptive fuzzy tracking control of MIMO switched nonlinear systems preceded by unknown backlash-like hysteresis," *Inf. Sci.*, vol. 490, pp. 369–386, Jul. 2019.
[35] L. Ma, G. Zong, X. Zhao, and X. Huo, "Observed-based adaptive finite-time tracking control for a class of nonstrict-feedback nonlinear systems with input saturation," *J. Franklin Inst.*, Sep. 2019, doi: 10.1016/j.jfranklin.2019.07.021.
[36] Y. Wang, W. Zhou, J. Luo, H. Yan, H. Pu, and Y. Peng, "Reliable intelligent path following control for a robotic airship against sensor faults," *IEEE/ASME Trans. Mechatronics*, vol. 24, no. 6, pp. 2572–2582, Dec. 2019.
[37] Y. Wang, H. R. Karimi, H.-K. Lam, and H. Yan, "Fuzzy output tracking control and filtering for nonlinear discrete-time descriptor systems under unreliable communication links," *IEEE Trans. Cybern.*, early access, Jun. 17, 2019, doi: 10.1109/TCYB.2019.2920709.
[38] D. Song, J. Yang, M. Dong, and Y. H. Joo, "Kalman filter-based wind speed estimation for wind turbine control," *Int. J. Control, Autom. Syst.*, vol. 15, no. 3, pp. 1089–1096, Jun. 2017.
[39] J. Yang, A. Zolotas, W.-H. Chen, K. Michail, and S. Li, "Robust control of nonlinear MAGLEV suspension system with mismatched uncertainties via DOBC approach," *ISA Trans.*, vol. 50, no. 3, pp. 389–396, Jul. 2011.
[40] F. L. Luo and R. Unbehaben, *Applied Neural Networks for Signal Processing*. Cambridge, U.K.: Cambridge Univ. Press, 1998.
[41] K.-H. Kim, T. L. Van, D.-C. Lee, S.-H. Song, and E.-H. Kim, "Maximum output power tracking control in variable-speed wind turbine systems considering rotor inertial power," *IEEE Trans. Ind. Electron.*, vol. 60, no. 8, pp. 3207–3217, Aug. 2013.
[42] K. H. Kim, D. C. Lee, and J. M. Kim, "Fast tracking control for maximum output power in wind turbine systems," in *Proc. AUPEC*, Dec. 2010, pp. 1–5.
[43] *GH bladed User Manual*, Garrad Hassan and Partners, Bristol, U.K., 2009.
[44] D. R. Song, Q. A. Li, Z. Cai, L. Li, J. Yang, M. Su, and Y. H. Joo, "Model predictive control using multi-step prediction model for electrical yaw system of horizontal-axis wind turbines," *IEEE Trans. Sustain. Energy*, vol. 10, no. 4, pp. 2084–2093, Oct. 2019.
[45] D. Song, J. Liu, J. Yang, M. Su, S. Yang, X. Yang, and Y. H. Joo, "Multi-objective energy-cost design optimization for the variable-speed wind turbine at high-altitude sites," *Energy Convers. Manage.*, vol. 196, pp. 513–524, Sep. 2019.
[46] D. Song, Y. Yang, S. Zheng, W. Tang, J. Yang, M. Su, X. Yang, and Y. H. Joo, "Capacity factor estimation of variable-speed wind turbines considering the coupled influence of the QN-curve and the air density," *Energy*, vol. 183, pp. 1049–1060, Sep. 2019.
[47] M. L. Corradini, G. Ippoliti, and G. Orlando, "Robust control of variable-speed wind turbines based on an aerodynamic torque observer," *IEEE Trans. Control Syst. Technol.*, vol. 21, no. 4, pp. 1199–1206, Jul. 2013.
[48] B. Boukhezzar and H. Siguerdidjane, "Nonlinear control of a variable-speed wind turbine using a two-mass model," *IEEE Trans. Energy Convers.*, vol. 26, no. 1, pp. 149–162, Mar. 2011.

XIAOFEI DENG received the B.S. degree in communication engineering from Jishou University, Jishou, China, in 2006, and the M.S. degree in control science and engineering from Central South University, Changsha, China, in 2009, where she is currently pursuing the Ph.D. degree.

Her research interests include advance control algorithms, soft computing technique and their application in systems of wind turbine and mobile robot.

JIAN YANG (Member, IEEE) received the Ph.D. degree in electrical engineering from the University of Central Florida, Orlando, FL, USA, in 2008.

He was a Senior Electrical Engineer with Delta Tau Data Systems, Inc., Los Angeles, CA, USA, from 2007 to 2010. Since 2011, he has been with Central South University, Changsha, China, where he is currently a Professor with the School of Information Science and Engineering. His main research interests include motion control, power electronics and its applications in wind energy generation systems, and photovoltaic systems.

YAO SUN (Member, IEEE) received the B.S., M.S., and Ph.D. degrees from Central South University, Changsha, China, in 2004, 2007, and 2010, respectively.

He has been a Full professor with the School of Automation, Central South University. His research interests include matrix converter, microgrid, and wind energy conversion systems.

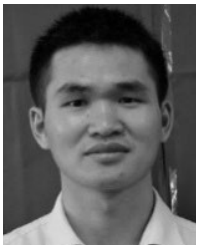

DONGRAN SONG received the B.S., M.S., and Ph.D. degrees in automation from the School of Information Science and Engineering, Central South University, Changsha, China, in 2006, 2009 and 2016, respectively.

He was an Electrical and Control Engineer with China Ming Yang Wind Power, Zhongshan, from 2009 to 2017. Since 2018, he has been with Central South University, where he is currently an Associate Professor with the School of Automation. His current research interests include advance control algorithms for wind turbines, power electronics, and renewable energy generation systems.

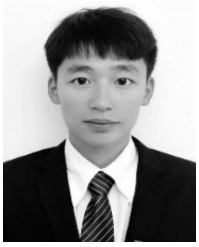

YINGGANG YANG received the B.S. degree in electrical engineering and automation from Central South University, Changsha, China, in 2019, where he is currently pursuing the M.S. degree in control science and engineering.

His research interest includes wind turbine control and its optimization.

YOUNG HOON JOO received the B.S., M.S., and Ph.D. degrees in electrical engineering from Yonsei University, Seoul, South Korea, in 1982, 1984, and 1995, respectively. He worked with Samsung Electronics Company, Seoul, from 1986 to 1995, as a Project Manager. He was with the University of Houston, Houston, TX, USA, from 1998 to 1999, as a Visiting Professor with the Department of Electrical and Computer Engineering. He is currently a Professor with the Department of Control and Robotics Engineering, Kunsan National University, South Korea. His major interests are mainly in the field of intelligent control, intelligent robot, human–robot interaction, wind-farm control, power system stabilization, and intelligent surveillance systems. He has served as the President for the Korea Institute of Intelligent Systems (KIIS), from 2008 to 2009. He has been serving as the Editor-in-Chief for the *International Journal of Control, Automation, and Systems* (IJCAS), since 2014, the Vice-President for the Korean Institute of Electrical Engineers (KIEE), since 2013, and for the *Institute of Control, Automation, and Systems* (ICROS), since 2016. Also, he has also been serving as the Director of Research Center of Wind Energy Systems funded by Korean Government, since 2016.